Radioprotection 49(2), 107-113 (2014)

DOI: 10.1051/radiopro/2013086

Available online at:
www.radioprotection.org

ARTICLE

Monte Carlo method used to determine scatter fractions for estimating secondary gamma-ray and X-ray photon dose equivalent rates

L. Bourgois[a] and N. Comte

CEA, DAM, DIF Bruyères-le-Châtel, 91297 Arpajon Cedex, France.

Received 21 June 2013 – Accepted 23 August 2013

Abstract – The Monte Carlo MCNPX code is used to calculate the scatter fraction, making it possible to assess the scattered dose equivalent rate. Two materials are considered for the phantom: water and steel. The calculations are performed by considering beams of monoenergetic photons (in the range 10 keV to 10 MeV) and bremsstrahlung photons resulting from the interaction of electrons (30–900 keV) on a tungsten target. The variation of the scatter fraction is investigated as a function of the primary photon energy, the beam area at the phantom surface, the scattering angle, and filtration of the bremsstrahlung radiation. We note the shortcomings of the ISO standard issued in 2011, which does not take into account the beam area at the phantom surface, the scattering angle or the scattering materials, thus producing inconsistencies with the computed values given in this study and in the literature. Our values for the scatter fraction are comparable with those given in the literature (*e.g.* NCRP). As regards the bremsstrahlung radiation, we note the influence of filtration, in particular at low energies. The scatter fractions given here are compatible with the calculation of the ambient dose equivalent, whereas in the literature, they are systematically used for the calculation of air kerma rates. We also obtain scatter fractions for water that are higher by a factor of 5 compared with steel.

Keywords: scattering / X-ray / Monte Carlo

1 Introduction

In the design of shielding for radiography facilities, it is important to estimate the radiation scattered (secondary dose) by a phantom (a patient in a medical diagnostic X-ray unit, or other objects in the path of the primary beam in an industrial facility). To calculate the secondary dose equivalent rate, $\dot{H}_{sec}$, scattered by a phantom, in a geometry such as that shown in Figure 1, certain authors (NCRP, 2005; Antoni and Bourgois, 2013a) use the following equation:

$$\dot{H}_{sec} = \frac{\dot{H}_0}{d_1^2}\frac{\alpha S}{d_2^2} \quad (1)$$

where: $\dot{H}_0$ is the dose equivalent rate due to the primary photon beam 1 m from the source (in the absence of a phantom), and $\frac{\dot{H}_0}{d_1^2}$ is the dose equivalent rate due to the primary beam on the surface of the phantom (with d_1 being the distance in metres between the source and the centre of the phantom), d_2 is the distance between the centre of the phantom and the observer (in m), S is the beam area at the phantom surface and α is the scatter fraction.

[a] Laurent.bourgois@cea.fr

The product αS is dimensionless and α has the reciprocal dimensions of S. By convention, S and α are taken as having the dimensions of cm^2 and cm^{-2}, respectively.

This equation is valid only for a sufficiently small beam area at the phantom surface with respect to the distance d_2, so the diffuse source can be regarded as a point with respect to the observer.

The scatter fraction (α) depends on the scattering angle θ, the energy of primary photon incident on the phantom and the material of the phantom.

Nevertheless, the method for calculating the secondary radiation given in a recent ISO standard NF C 15-160 (2011) fails to take into account the beam area at the phantom surface or the nature of the phantom, and does not consider the variation of the scatter fraction according to the scattering angle.

The values for the scatter fraction, α, available in the literature (NCRP, 1976; Simpkin and Dixon, 1998; NCRP, 2005) have been used to estimate the scattered air kerma rate and not the ambient dose equivalent rate as proposed here. Moreover, since these studies are concerned with medical applications, the scattering material in question consists only of water and the energies involved are limited.

The present study uses a Monte Carlo code to calculate the variation of the secondary dose equivalent rate as a function of the beam area at the phantom surface and the scattering

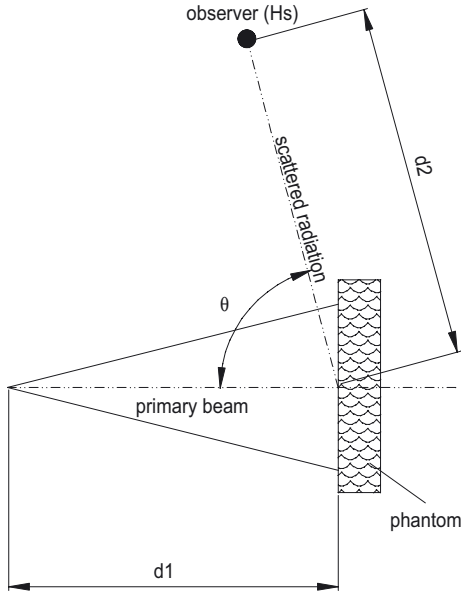

Fig. 1. Geometry considered for equation (1).

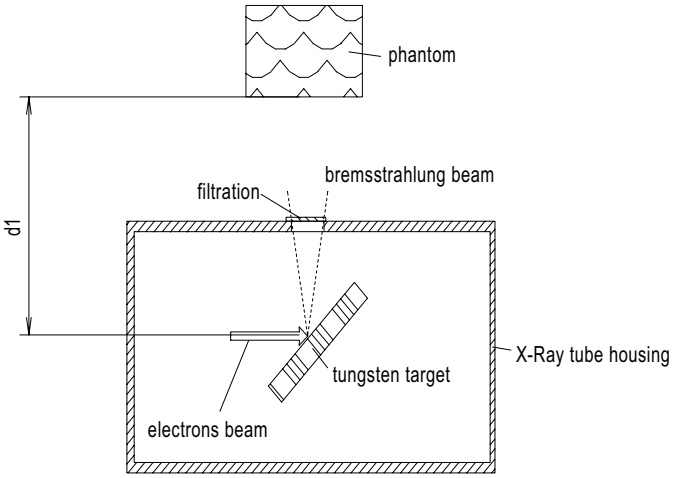

Fig. 2. Geometry considered for bremsstrahlung photons.

angle. The photons considered here are monoenergetic beams (10 keV to 10 MeV), or result from bremsstrahlung radiation due to the interaction of electrons (30–900 keV) on a tungsten target. The phantom materials considered are water and steel.

2 Materials and method

Calculations are based on the Monte Carlo code MCNPX version 2.5.0 (Pelowitz, 2005). The effective cross-sections used here are taken from mcplib04 of the library ENDF/B-VI Release 8 (White, 2002). Calculations are performed to obtain the ambient dose equivalent at a depth of 10 mm: $H^*(10)$. For this purpose, we determine the photon fluence at a point by means of a type-5 tally in mode p (in this case the "Thick Target Bremsstrahlung model" – TTB – is used), weighted by the coefficients used to convert fluence to the ambient dose equivalent at 10 mm as published by the ICRU (1998). Statistical tests on the whole set of calculations are in conformity with the results expected for a type-5 tally.

The geometry considered here is presented in Figure 1, with the distances d_1 and d_2 being equal to 1 m. The primary photons are emitted from the source in a cone with an adjustable apex angle, making it possible to vary the beam area at the phantom surface. In this configuration, the area is limited to 400 cm^2 (disc of radius 11.3 cm), so this secondary source, which has a disc-type geometry, can be considered as a point with respect to the observer (Antoni and Bourgois, 2013b).

The simulated phantom is a cylinder of water or steel with a section of 450 cm^2 and a length of 100 cm.

To calculate the results for an X-ray generator, the bremsstrahlung photons are simulated by the Monte Carlo code using the interaction of a beam of electrons of kinetic energy T on a tungsten target (45° target angle). For these calculations the case is split into two parts: first of all, electrons on the target for generating the photon spectrum (MCNPX mode p e in this case), and second of all, the photon distribution put as a source (MCNPX mode p with the TTB model in this case). The electron beam is parallel. Filtration of the bremsstrahlung photons is also simulated to explore the influence of this parameter on the value of the scatter fraction α. We should point out that the X-ray tube housing is "perfect", *i.e.* any particle arriving at this X-ray tube housing is no longer considered by the transport code. The geometry of the unit is shown in Figure 2.

3 Results

3.1 Variation of the equivalent dose due to secondary radiation, as a function of the beam area at the phantom surface

Figure 3 shows the variation of the ratio $\frac{\dot{H}_{sec}}{\dot{H}_0}$ as a function of the beam area at the phantom surface S, assuming a water-scattering phantom, for photons in the energy range 100 keV to 1 MeV and at various angles θ.

We note that the ratio $\dot{H}_{sec}/\dot{H}_0$ is proportional to the beam area at the phantom surface, with a statistical variability of less than 10% for a linear interpolation between 1 and 400 cm^2.

The dose equivalent rate arising from secondary radiation thus shows a good linear correlation with the beam area at the phantom surface. Equation (1) is thus validated.

In the following calculations, we assume a beam area at the phantom surface of 200 cm^2. To facilitate comparison of the results, the scatter fraction α is normalised to a beam area at the phantom surface of 1 cm^2.

3.2 Scatter fractions α for monoenergetic photons

Figures 4 and 5 give the values of the scatter fraction calculated by the MCNPX Monte Carlo code for monoenergetic photons scattered in various directions by a water and steel phantom, respectively. The calculated values are normalised to a beam area at the phantom surface, S, of 1 cm^2.

Figure 4 shows that, for a water phantom and with monoenergetic photons of energy ranging between 10 keV and

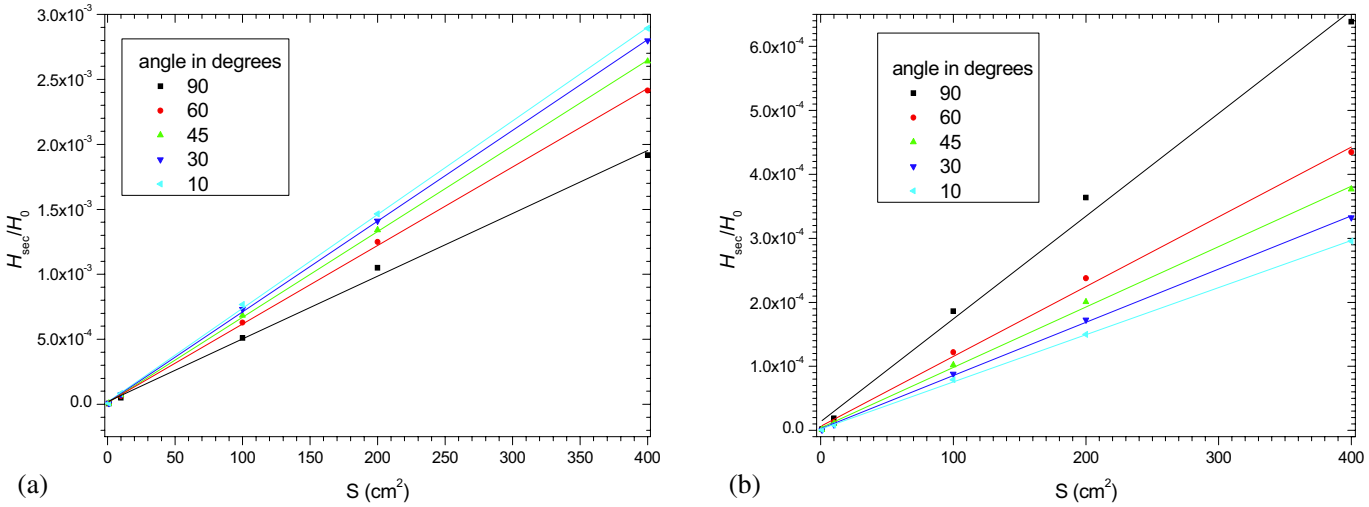

Fig. 3. Variation of the ratio $\dot{H}_{sec}/\dot{H}_0$ as a function of beam area at the phantom surface S, for photons of energy 100 keV (a) and 1 MeV (b). The data points represent the results of calculations, and the lines indicate a linear interpolation of the calculated points.

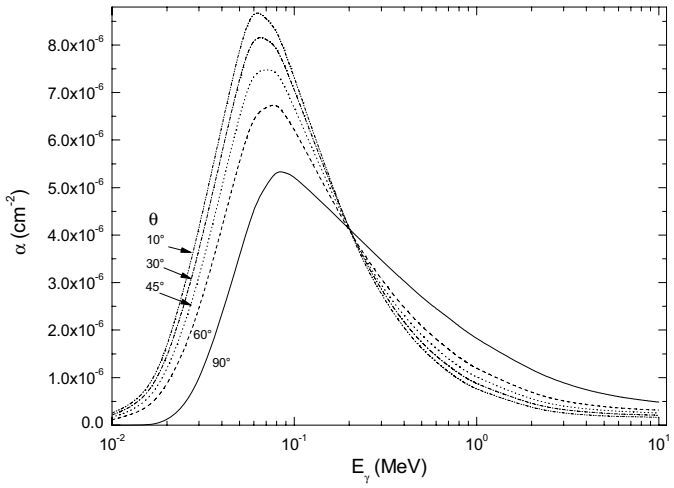

Fig. 4. Scatter fraction as a function of energy of monoenergetic photons (10 keV to 10 MeV) at various scattering angles (ranging from 10° to 90°) for a water phantom.

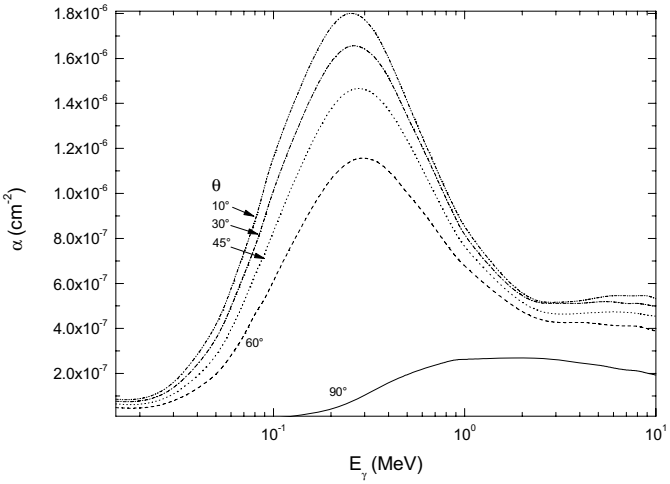

Fig. 5. Scatter fraction as a function of energy of monoenergetic photons (15 keV to 10 MeV) at various scattering angles (ranging from 10° to 90°) for a steel phantom.

200 keV, the scatter fraction increases with a decreasing scattering angle θ. The reverse tendency is observed for photon energies higher than 200 keV. The maximum scatter fractions are obtained at a scattering angle θ of 10° for photon energies of about 60 keV, with θ ranging up to 90° at 80 keV.

Figure 5 shows that, for a steel phantom and with monoenergetic photons of energy ranging between 10 keV and 10 MeV, the scattering angle θ decreases with an increasing α coefficient. The maximum scatter fraction is obtained at a scattering angle θ of 10° for photon energies of about 200 keV, with θ ranging up to 60° at 300 keV. It should be noted that low scatter fractions are obtained at an angle of 90°. This is due to the phantom design, which presents a significant attenuation for this angle, in particular with a steel phantom.

It is also noteworthy that the value of the scatter fraction is higher by a factor of 5 for a scattering phantom composed of water compared with steel.

3.3 Scatter fraction α for bremsstrahlung photons without filtration

Figures 6 and 7 give the values of the scatter fraction calculated by the MCNPX Monte Carlo code for bremsstrahlung photons resulting from the interaction of electrons of kinetic energy T on a tungsten target, which are then scattered in various directions by a water and steel phantom, respectively. The calculated values are normalised to a beam area at the phantom surface, S, of 1 cm^2.

For a phantom composed of water or steel and a bremsstrahlung X-ray spectrum resulting from the interaction of electrons on a tungsten target, with kinetic energies ranging from 30 keV to 900 keV, Figures 6 and 7 show that the scatter fraction increases with a decreasing scattering angle θ. For a water phantom, the maximum values of the scatter fraction are obtained at a scattering angle θ of 10° for an electron energy of about 300 keV, and at θ = 90° for 700 keV. For a steel phantom, the maximum values of the scatter fraction are obtained

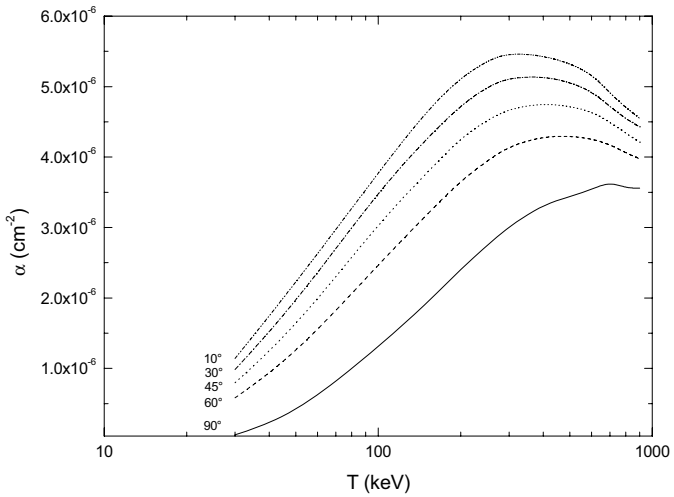

Fig. 6. Scatter fraction as a function of scattering angle (ranging from 10° to 90°) for bremsstrahlung photons resulting from the interaction of electrons (kinetic energy ranging from 30 to 900 keV) on tungsten, without filtering, for a water phantom.

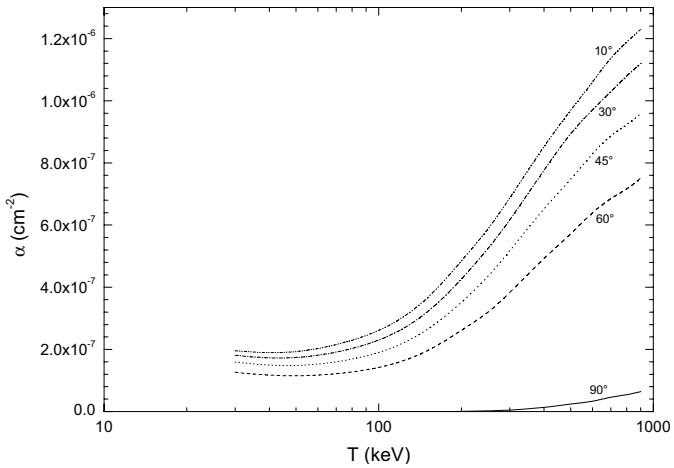

Fig. 7. Scatter fraction as a function of scattering angle (ranging from 10° to 90°) for bremsstrahlung photons resulting from the interaction of electrons (kinetic energy ranging from 30 to 900 keV) on tungsten, without filtering, for a steel phantom.

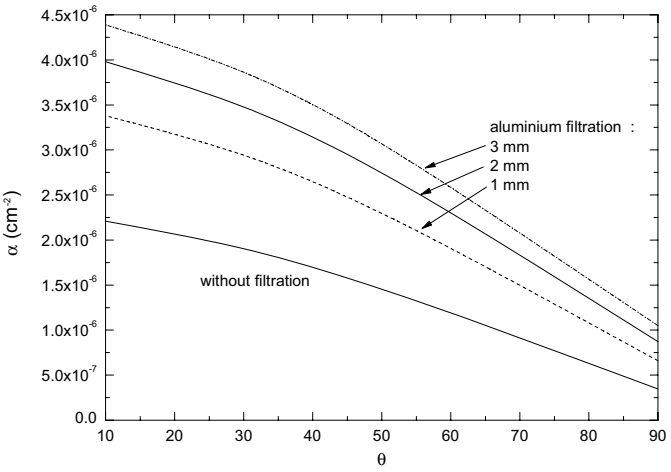

Fig. 8. Scatter fraction as a function of scattering angle (ranging from 10° to 90°) for bremsstrahlung photons resulting from the interaction of electrons (kinetic energy = 50 keV) on tungsten, for various filters and a water phantom.

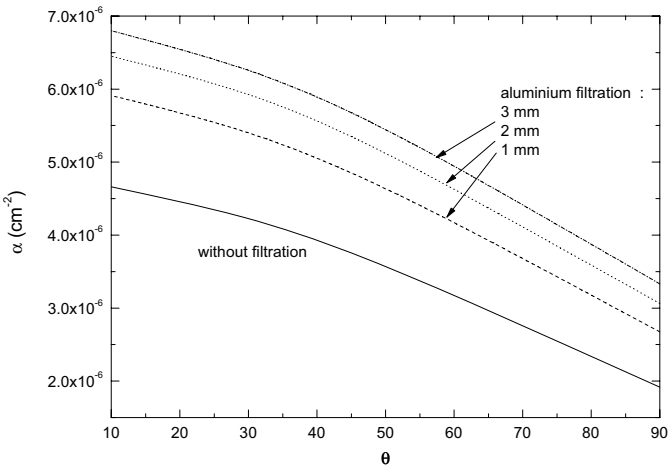

Fig. 9. Scatter fraction as a function of scattering angle (ranging from 10 to 90°) for bremsstrahlung photons resulting from the interaction of electrons (kinetic energy = 150 keV) on tungsten, for various filters and a water phantom.

at the maximum energy of electrons assumed in this study, *i.e.* 900 keV.

3.4 Scatter fraction α for bremsstrahlung photons with filtration

3.4.1 Water phantom

Figures 8, 9 and 10 give the values of the scatter fraction calculated by the MCNPX Monte Carlo code. The bremsstrahlung photons result from the interaction of electrons (with kinetic energy T = 50, 150 and 600 keV) on a tungsten target, which are then scattered in various directions by a water phantom. The scatter fractions are calculated for filtration thicknesses of 1, 2 and 3 mm of aluminium. The values shown here are normalised to an irradiated surface, S, of 1 cm^2.

For bremsstrahlung radiation resulting from the interaction of electrons with a kinetic energy of 50 keV on a tungsten target (Fig. 8), increasing the filtration thickness leads to a higher scatter fraction. Thus, for example, for a scattering angle of 10°, the scatter fraction for a spectrum filtration with 3 mm of aluminium is twice as high compared with the value obtained for an unfiltered spectrum. This is due to the fact that the mean energy of the spectrum increases with the thickness of filtration. This is in agreement with our findings for monoenergetic photons with kinetic energies in the range 20 to 50 keV; the value of the scatter fraction increases with energy (see Fig. 4).

The variation is identical for a spectrum resulting from the interaction of electrons with a kinetic energy of 150 keV (Fig. 9), but the influence of filtration is less important at this energy when the aluminium filtration is less than 3 mm thick. Thus, for a scattering angle of 10°, the scatter fraction for a

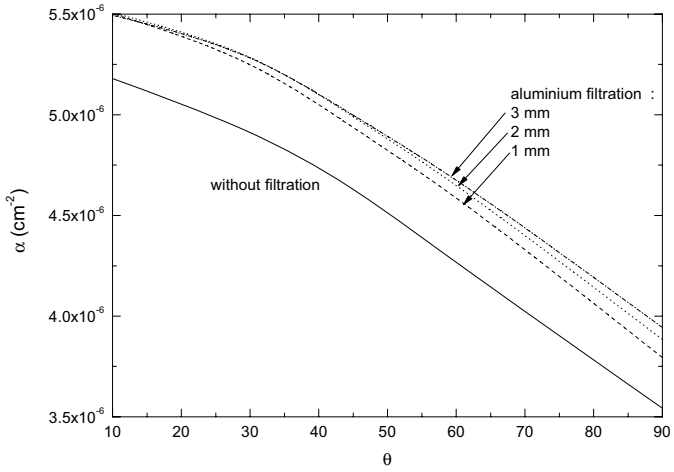

Fig. 10. Scatter fraction as a function of scattering angle (ranging from 10° to 90°) for bremsstrahlung photons resulting from the interaction of electrons (kinetic energy = 600 keV) on tungsten, for various filters and a water phantom.

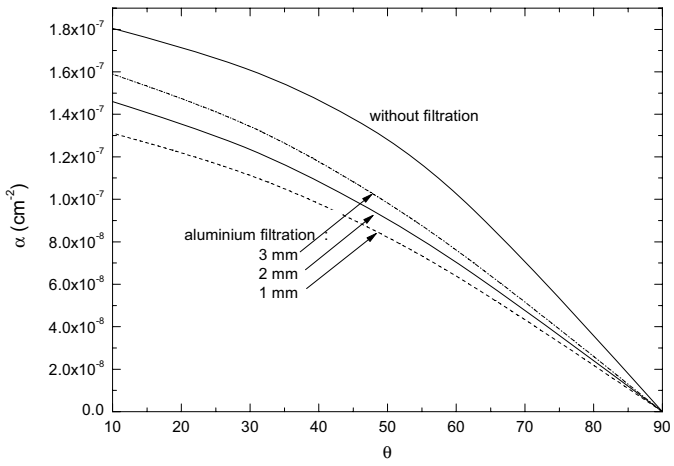

Fig. 11. Scatter fraction as a function of scattering angle (ranging from 10° to 90°) for bremsstrahlung photons resulting from the interaction of electrons with a kinetic energy of 50 keV on tungsten, with various filters, for a steel phantom.

spectrum filtered with 3 mm of aluminium is 50% higher compared with the value obtained for an unfiltered spectrum.

At 600 keV (Fig. 10), filtration with less than 3 mm of aluminium has almost no influence on the value of the scatter fraction. With a spectrum filtered by 3 mm of aluminium, the scatter fraction is only 6% higher compared with the value obtained for an unfiltered spectrum.

3.4.2 Steel phantom

Figures 11, 12 and 13 give the values of the scatter fraction calculated by the MCNPX Monte Carlo code. The bremsstrahlung photons result from the interaction of electrons of kinetic energy T = 50, 150 and 600 keV on a tungsten target, which are then scattered in various directions by a steel phantom. The values of the scatter fraction are given

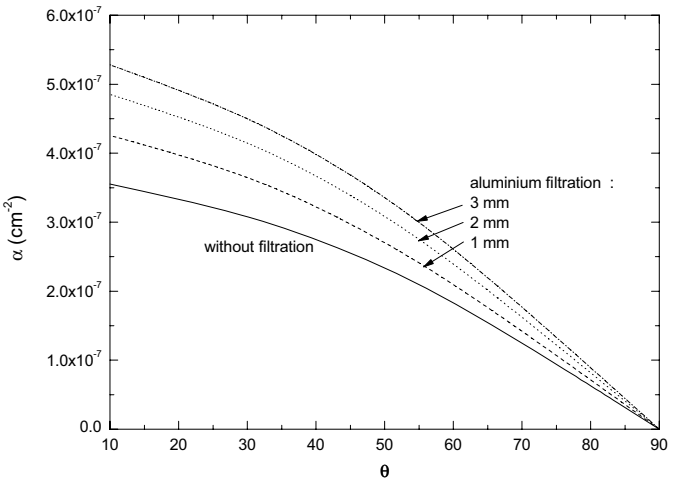

Fig. 12. Scatter fraction as a function of scattering angle (ranging from 10° to 90°) for bremsstrahlung photons resulting from the interaction of electrons with a kinetic energy of 150 keV on tungsten, for various filters and a steel phantom.

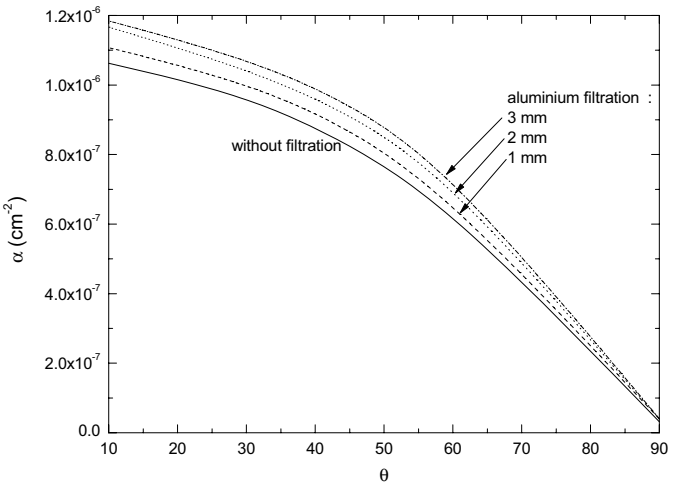

Fig. 13. Scatter fraction as a function of scattering angle (ranging from 10° to 90°) for bremsstrahlung photons resulting from the interaction of electrons with a kinetic energy of 600 keV on tungsten, for various filters and a steel phantom.

for various thicknesses of aluminium filtration. The calculated values are normalised to an irradiated surface, S, of 1 cm^2.

For a steel phantom, we can draw the same conclusions as in the case of a water phantom. We also note that the scatter fraction is higher for a water phantom than for steel. Nevertheless, for bremsstrahlung photons produced by electrons of kinetic energy equal to 50 keV, the scatter fraction for a filtered spectrum is smaller compared with the value obtained for an unfiltered spectrum.

4 Discussion

To compare our results with the literature, Table 1 reports the values of the scatter fraction for a beam area at the phantom surface of 1 cm^2 (except ISO (2011)) and for a bremsstrahlung

Table 1. Values of scatter fraction for a beam area at the phantom surface of 1 cm^2, compiled from various publications. The scattering angle considered here is 60° (except ISO, 2011), for bremsstrahlung photons resulting from the interaction of electrons on a tungsten target and in the case of a water phantom.

T (keV)[1]	NCRP (2005)[2] (cm^{-2})	NCRP (1976)[3] (cm^{-2})	Simpkin and Dixon (1998)[3] (cm^{-2})	Noto *et al.* (2009) (cm^{-2})[4]	ISO (2011)[5]	This study, with 3-mm-thick Al filtration (cm^{-2})	This study, without filtration (cm^{-2})
30	4.7×10^{-6}						5.8×10^{-7}
50	5.1×10^{-6}	2.00×10^{-6}	1.90×10^{-6}	3.3×10^{-6}	1.00×10^{-3}	2.3×10^{-6}	1.2×10^{-6}
100	5.9×10^{-6}	5.00×10^{-6}	4.90×10^{-6}	5.1×10^{-6}	2.20×10^{-3}	4.3×10^{-6}	2.5×10^{-6}
150	6.7×10^{-6}	6.00×10^{-6}	5.80×10^{-6}	5.9×10^{-6}	2.60×10^{-3}	4.6×10^{-6}	3.2×10^{-6}
200		6.75×10^{-6}			2.80×10^{-3}		3.7×10^{-6}
250		6.75×10^{-6}			2.80×10^{-3}		3.9×10^{-6}
300		6.50×10^{-6}			2.80×10^{-3}	5.1×10^{-6}	4.2×10^{-6}

[1] Kinetic energy of the electrons.
[2] This reference does not propose a discrete value for the scatter fraction, but a polynomial (3rd degree for θ and 1st degree for T) interpolation of various values in the literature allows us to calculate this coefficient between 30 and 150 keV. X-rays are filtered. Scatter fractions are in terms of kerma.
[3] For these references, X-rays are filtered by aluminium (0.5 mm to 2.5 mm thick, according to energy). Scatter fractions are in terms of kerma.
[4] For these references, X-rays are filtered by 2.5 mm aluminium. Scatter fractions are in terms of kerma.
[5] This reference omits any mention of irradiated surface values, the variation in θ, the nature of the scattering material or X-ray filtering. The values shown here are thus reproduced as given in the standard. N.B. in the standard, this quantity has the dimensions of m^2. Scatter fractions are in terms of dose equivalent.

spectrum. For the purposes of this comparison, we only include data collected using a scattering angle of 60° (except ISO (2011), no angle specified) and a water phantom (except ISO (2011), no material specified). The bremsstrahlung photons result from the interaction of electrons on tungsten.

Because the ISO standard (2011) does not take into account the beam area at the phantom surface, the scattering angle or the nature of the scattering material, it seems difficult to compare their values with those of the literature. Also, it is important that the assumptions used in the standard are mentioned.

Apart from the values given by the ISO (2011), the highest values listed in this table are from the NCRP (2005). Noto *et al.* (2009), also observed this overestimate compared with their own measurements (the NCRP (2005), values are higher by a factor of 1.3 to 3 for an X-ray tube at 70 kV). It should be pointed out that the values of the NCRP (2005), result from an interpolation of various values from the literature for kinetic energies between 30 and 150 keV. This interpolation is based on a 3rd degree polynomial for θ and a 1st degree polynomial for kinetic energy.

The computed values presented here are of the same order of magnitude as those given by the NCRP (1976), and Simpkin and Dixon (1998). It should be emphasised that our ratio values are calculated in terms of the quantity $H^*(10)$, whereas the other values listed in Table 1 are measured in terms of kerma. This explains the slight underestimation of our values compared with the literature.

5 Conclusion

Most available scatter fraction data published in the literature result from the medical field such as medical X-ray imaging facilities, thus the energy range and the phantom material are restricted. To complete the data published in the literature, we used a Monte Carlo code to calculate the scatter fraction in terms of the ambient dose equivalent rate, investigating its variation as a function of the beam area at the phantom surface and the scattering angle for monoenergetic photons with kinetic energies of 10 keV to 10 MeV, and for bremsstrahlung photons resulting from the interaction of electrons with energies ranging from 30 keV to 900 keV on a tungsten target. Water and steel are considered as scattering materials. Thus, in addition to the medical field, these data can also perform calculations in the industrial field (gammagraphy, industrial X-ray radiography).

Comparatively, our values are of the same order of magnitude as those available in the literature. We note the influence of filtration, in particular at low energies. It should be stressed that our scatter fraction values are given with the same dimensions as the ambient dose equivalent rate, whereas, in the literature, they are systematically given for the calculation of air kerma. It should be noted that our results, in terms of the quantity "ambient dose equivalent", are more adapted than "kerma" for radiological zoning or shielding design.

We also point out that water exhibits a fivefold higher scattering compared with steel.

Nevertheless, because the ISO standard (2011), does not take into account the beam area at the phantom surface, the scattering angle or the nature of the scattering material, it seems difficult to compare their values with those of the literature. Also, it is important that the assumptions used in the standard are mentioned. This generates inconsistencies with the computed values of the scatter fraction presented here and in the literature.

References

Antoni R., Bourgois L. (2013a) Principes généraux de protection contre l'exposition externe. In: *Physique appliquée à l'exposition externe : dosimétrie et radioprotection*. Springer, Paris.

Antoni R., Bourgois L. (2013b) Grandeurs et unités fondamentales de la dosimétrie externe. In: *Physique appliquée à l'exposition externe : dosimétrie et radioprotection*. Springer, Paris.

ICRU Report 57 (1998) *Conversion coefficients for use in radiological protection against external radiation*. Pergamon Press, Oxford.

ISO Norme NF C 15-160 (2011) Installation pour la production et l'utilisation de rayonnements X – Exigences de radioprotection.

NCRP Report 49 (1976) National Council on Radiation Protection and Measurements Structural Shielding Design and evaluation for Medical use of X-Rays and Gamma-Rays up to 10 MeV.

NCRP Report 147 (2005) National Council on Radiation Protection and Measurements Structural Shielding Design for Medical X-Ray Imaging Facilities.

Noto K., Koshida K., Iida H., Yamamoto T., Kobayashi I., Kawabata C. (2009) Investigation of scatter fractions for estimating leakage dose in medical X-ray imaging facilities, *Radiol. Phys. Technol.* **2**, 138-144.

Pelowitz D.B. (2005) MCNPX user's manual LA-CP-05-369.

Simpkin D.J., Dixon R.L. (1998) Secondary shielding barriers for diagnostic X-Ray facilities : scatter and leakage revisited, *Health Phys*. **74** (3), 350-365.

White M.C. (2002) Photoatomic data library MCPLIB04: a new photoatomic library based on data from ENDF/B-VI release 8. Los Alamos National Laboratory Memorandum No. X-5:MCW-02-111.

Cite this article as: L. Bourgois, N. Comte. Monte Carlo method used to determine scatter fractions for estimating secondary gamma-ray and X-ray photon dose equivalent rates. Radioprotection 49(2), 107-113 (2014).